SIMULATION OF FLOW AND TEMPERATURE DEVELOPMENT IN A THERMOACOUSTIC RESONATOR

Kim Fa Liew[1], Normah Mohd-Ghazali[1*]

[1]*Faculty of Mechanical Engineering, University of Technology Malaysia, Johor Bahru, 81310, Johor, Malaysia*

ABSTRACT

The fluid flow pattern in a thermoacoustic resonator is an important characteristic that affects the performance of the thermoacoustic refrigerator. The main factor that affects the flow and subsequently the heat transfer processes between the oscillating fluid and the stack walls is the geometry of the stack unit, especially related to the stack thickness and stack separation. In this paper, a two-dimensional numerical simulation of the inviscid fluid flow around the stack unit in a quarter wavelength resonator is carried out by using the continuity, Navier-Stokes, energy and ideal gas equations. These equations are solved using the perturbation method and the finite difference method. Three cases of different stack plate thickness are investigated: negligible, 0.4 mm and 0.8 mm thicknesses, respectively. The stack separation has also been varied for the 0.4 mm thickness, within and beyond that recommended by previous studies. Results show that vortices and streaming are always present, more significantly with the thicker plates. Concentrated vortices in the thick plate case stay longer than those with the thinner plate. They contribute to the high heat transfer rate as shown by the temperature profiles.

Keywords: Numerical simulation; Stack plate; Streaming; Thermoacoustic; Vortices

1. INTRODUCTION

Thermoacoustic refrigeration is a relatively new technology that gained attention of researchers several decades ago, due to its environmentally friendly system. Without the use of any refrigerants or a compressor, acoustic energy is converted into heat energy through the oscillatory motions of the working fluid. As these particles pass by solid walls within a stack unit, which usually consists of a bundle of plates, a temperature gradient develops and is maintained when the ends of the stack unit are connected to a heat source (load) and a heat sink (atmosphere). Two types of thermoacoustic cooling are possible, but the standing wave thermoacoustic refrigerator is studied here because it takes up a smaller space compared to the travelling wave system. As fluid particles in an enclosure get adiabatically compressed, the temperature rises (without any gain or loss in heat), becoming higher than the neighboring solid walls. Heat is transferred from the fluid to the walls, lowering its temperature. During the next cycle, as the fluid expands (without any loss or gain in heat), its temperature is much lower than the neighboring wall because the wall which has gained some heat energy from a previous batch of fluid particles. Heat is transferred from the walls to the fluid particles. The system is similar to a line of firemen passing buckets of water to cool the walls. However, much of the thermoacoustic cooling effects are still unknown with theories still being developed to explain the phenomena.

The first numerical simulation of the thermoacoustic effects was conducted by Cao et al. (1996). The continuity, momentum, and energy equations were solved on an isothermal negligible thickness parallel plate in a standing wave resonator with the SOLA-ICE method. In the same year, Worlikar and Knio (1996) simulated a two-stack configuration of a thermoacoustic refrigerator using the numerical finite difference method with the same equations as Cao et al. (1996) but with a low Mach number model. They varied their simulation with different drive ratios, blockage ratios, and stack separation to plate thickness ratios, and stack positions. Their work, however, omitted the presence of the oscillating conditions surrounding the stack. The first simulation completed on the whole resonator was probably done by Mohd-Ghazali (2001), where many complexities have been observed, including mode competition, vortex shedding and other non-linear effects. The data were taken right after the acoustic waves hit the solid walls of the stack. The numerical simulation work is continued by Ishikawa and Mee (2002), and Zoontjens et al. (2009) by introducing a longer stack length and non-zero thickness plate respectively. Zoontjens et al. utilized the commercial CFD package, FLUENT to model the behavior of flow near a single plate. In these studies, vortices have been observed between the plates as well as near the edges. The vortex patterns have been studied by several researchers. Blanc-Benon et al. (2003) studied numerically and experimentally the sizes of the vortices at the ejection end. Using the particle image velocimetry method (PIV), Shi et al. (2010) classified the vortex motion recorded around the stack unit into eight patterns, which include symmetrical vortices relative to the plate or channel, a merging vortex and an alternate shedding vortex. Zhang et al. (2013) also studied experimentally the flow around a parallel stack unit with PIV with various drive ratios. The streaming effect reported in past studies is an important factor in the thermoacoustic phenomena where momentum losses could occur significantly and reduce the desired cooling intended. Galioulinna et al. (2005) investigated numerically and analytically the secondary streaming in the resonator. Abd El-Rahman and Abdel-Rahman (2013) found that streaming effects become significant when the drive ratio is large.

So far, numerical studies on the region surrounding the stack plate(s) have not comprehensively looked at the velocity and temperature profiles in association with the vortex development and streaming effects surrounding the stack. This paper reports the simulation study of the oscillating fluid flow that surrounds the stack unit of a standing wave thermoacoustic resonator, using the finite difference method. The system of algebraic equations is solved with a MATLAB code developed for that purpose. A single plate and a double plate computational domain, with different thickness and separation gaps are considered.

2.   METHODOLOGY

2.1.   Governing Equations
The working fluid is an ideal gas confined in an adiabatic system. The two-dimensional flow in *x*- and *y*-direction is modeled as a Newtonian fluid which is incompressible, unsteady, and inviscid. The last assumption was made based on an earlier simulation, which showed insignificant differences with the viscous model (Liew, 2015). The thermo properties are constants at 298K, with body forces neglected. With all these assumptions, the governing equations are the conservation of mass,

$$\frac{\partial \rho}{\partial t} + \nabla \cdot (\rho \boldsymbol{u}) = 0$$

$$(1)$$

the Navier-Stokes equation,

$$\rho \frac{Du}{Dt} = -\nabla p \tag{2}$$

and the energy equation,

$$\rho c_p \frac{DT}{Dt} = \nabla \cdot (k \nabla T) + \frac{Dp}{Dt} \tag{3}$$

Equations (1) through (3), together with the ideal gas equation, $p = \rho RT$, are transformed into algebraic forms using finite difference with the accuracy of $O(h^2)$. Term ρ is the fluid density, u represents the horizontal and vertical velocity, u and v, c_p is the fluid constant pressure specific heat, k is the fluid thermal conductivity, p is the pressure, T is the temperature and R is the gas constant per unit mass. Due to compression and expansion, the density, pressure, and temperature are defined as (Mohd-Ghazali, 2001),

$$p = p_m + p' \tag{4}$$

$$\rho = \rho_m + \rho' \tag{5}$$

$$T = T_m + T' \tag{6}$$

The p_m, ρ_m and T_m terms are the constants, their values taken as 101.325kPA, 0.1637 kg/m³, and 298K, respectively. The p', ρ' and T' are the fluctuating parts to be determined. Subsequently, all the fluctuating terms henceforth are used without the "tick". The Boussinesq approximation is applied and the formulated equations are then solved using a self-developed MATLAB code.

2.2. Computational Domain

Figure 1 shows the physical domain of the thermoacoustic resonator. The overall length or the resonator, L, is 0.635 m, which is $\lambda/4$, λ being the wavelength. The stack center position from the driver end, x_c, is 0.09 m ($\approx \lambda/25$). The region within the dashed line is the computational domain, which has a length of 0.250 m. Its height is set according to the stack thickness, d, and the stack separation, h, both of which are important parameters and both of these parameters are related with blockage ratio (Setiawan et al., 2013).
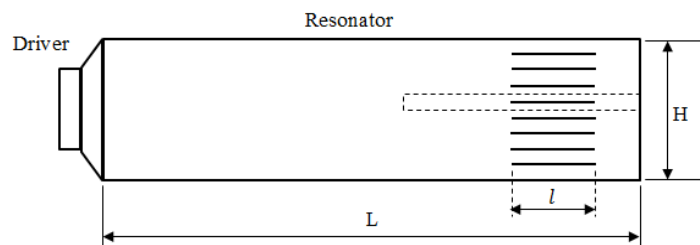
Figure 1 Physical domain of the thermoacoustic resonator

Figures 2 and 3 show the computational domain of a single plate and double plate configurations. The boundary conditions of the computational domain are:

AC $: u = u_o \sin(\omega t), v = 0, T = T_m$

BD $: u = 0, v = 0, \frac{\partial T}{\partial x} = 0$

EF $: u = 0, v = 0, T = T_m$

AB and CD (symmetric boundary conditions) $: \frac{\partial}{\partial y} u = 0, v = 0, \frac{\partial T}{\partial y} = 0$
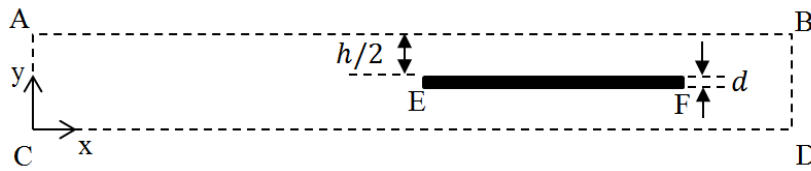
Figure 2 Computational domain of a single plate configuration
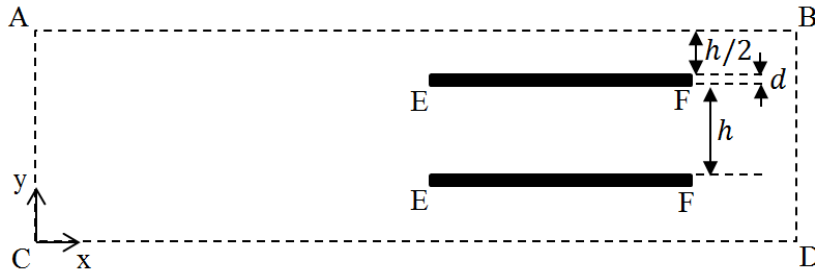
Figure 3 Computational domain of a double plate configuration

The model follows that of Tijani's physical system (Tijani, 2001), the working gas used being Helium at the operating frequency of 400 Hz. The Drive Ratio, DR, which is defined as the ratio of pressure amplitude to the system pressure is set at 0.5%. With the relation of velocity amplitude to the pressure amplitude, 3 m/s is determined to be used as the velocity amplitude, u_o. The length of the stack and the stack separation are 95 mm and 2 mm, respectively. The cases investigated are shown in Table 1, where Br is the blockage ratio, the percentage of stack separation (porosity) over the stack distance which defined as:

$$Br = \frac{h}{h+d}$$

(5)

Table 1 Parametric study of the stack thickness to the flow pattern

Case	No. of plate	d (mm)	h (mm)	Br
1	1	0.4	2.0	0.83
2	1	0.0	2.0	1.00
3	1	0.8	2.0	0.71
4	2	0.4	2.0	0.83
5	2	0.0	2.0	1.00
6	2	0.8	2.0	0.71
7	2	0.4	1.6	0.80
8	2	0.4	1.2	0.75

3.   RESULTS AND DISCUSSION

To show the flow patterns around a single plate of the parallel stack unit, the computed velocity around the stack unit is shown in vector plots and streamlines for the three cases investigated. Figure 4 shows the plots for the 0.4 mm thickness plate at two different time frames; both plots are taken after the initial wave front hits the end wall, before the half cycle (7T/16) and at half cycle (T/2). Due to the finite thickness and length of the plate, streaming and edge effects are observed. The streaming is not so conspicuous until the half cycle, probably due to the

relatively large computational grid imposed, spatially and temporally. Nonetheless, the development of the double vortices can be seen clearly. Streaming effects between the plates can barely be detected at the half cycle. The phenomena has been reported in previous numerical studies (Ishikawa & Mee, 2002; Marx & Blanc-Benon, 2004; Worlikar & Knio, 1996). Worlikar and Knio only looked at the flow effects between the parallel stack plates without propagating the wave boundary conditions. Meanwhile, Marx and Blanc-Benon investigated a zero thickness plate.
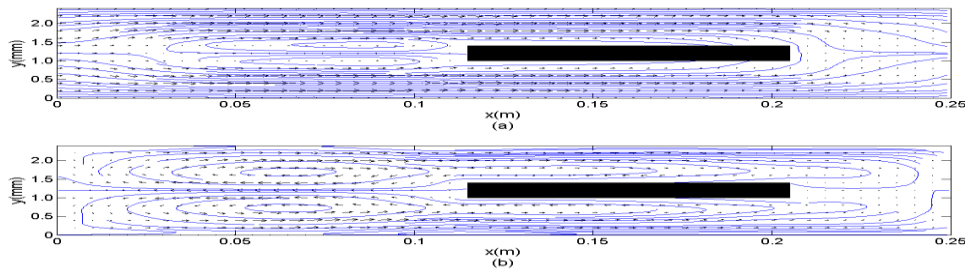
Figure 4 Vector plot and streamline for Case 1 at (a) 7T/16 and (b) 8T/16

Figure 5 shows the vector plots and streamlines of the flow around the zero thickness stack plate. There is no formation of the vortex before the half cycle as seen in Figure 4(a). Elongated vortices do appear during the half cycle and they disappear later.
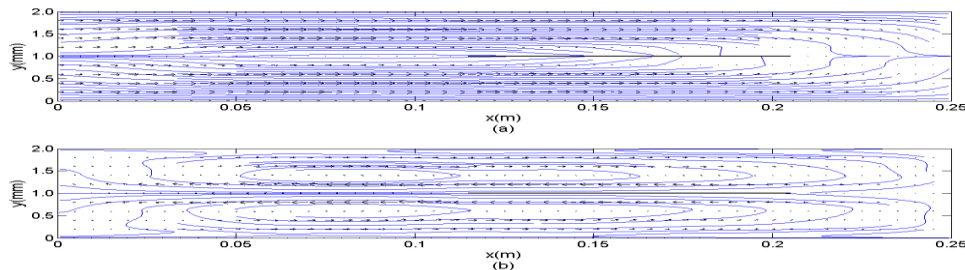
Figure 5 Vector plot and streamline for Case 2 at (a) 7T/16 and (b) 8T/16

Figure 6 shows the vector plots and streamlines of the flow around the 0.8 mm thickness stack, twice the thickness of Case 1. It has similar flow patterns where the vortices form before the half cycle and become larger during the half cycle as shown in Figures 5(a) and 5(b). The significant corners caused higher vertical components of the velocity and the disappearance of vortices is much more difficult to observe. Streaming in the gap, as well as at the far end at half cycle can be seen here.
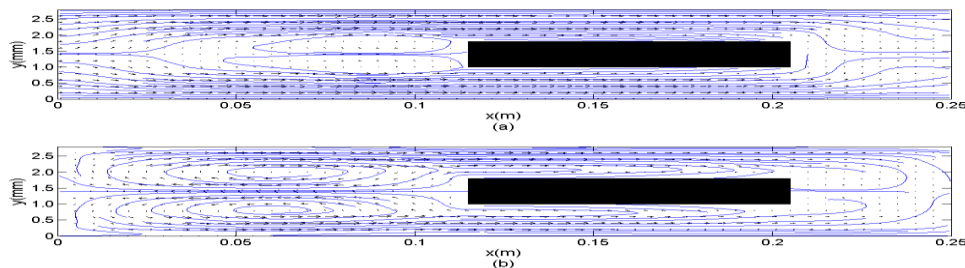
Figure 6 Vector plot and streamline for Case 3 at (a) 7T/16 and (b) 8T/16

The only similarity of the runs is that the vortical motion is stronger at the left end than that at the right end of the stack. This is similar to most of the previous results (Abd El-Rahman &

Abdel-Rahman, 2013; Zhang et al., 2013). These results also agree with the Blanc-Benon et al. (2003) results with an elongated vortex for the thin plate, while concentrated vortex happens with the thick plate. As determined by Knio and Worlikar, a thicker stack plate resulted in a larger number and size of vortices near the plate, while a smaller separation gap discouraged the development of elongated streaming effects. To understand better the relationship between the flow pattern and the presence of plates, the simulation was completed for a two-plate region, shown here in Figures 7 through 9.
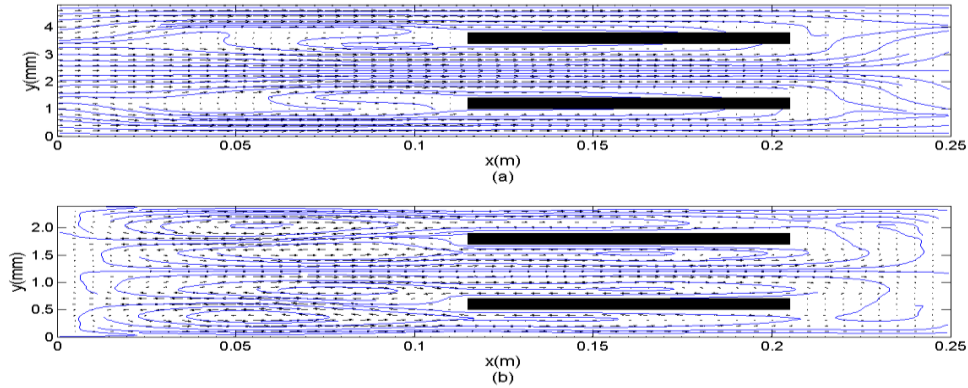
Figure 7 Vector plot and streamline for Case 4 at (a) 7T/16 and (b) 8T/16
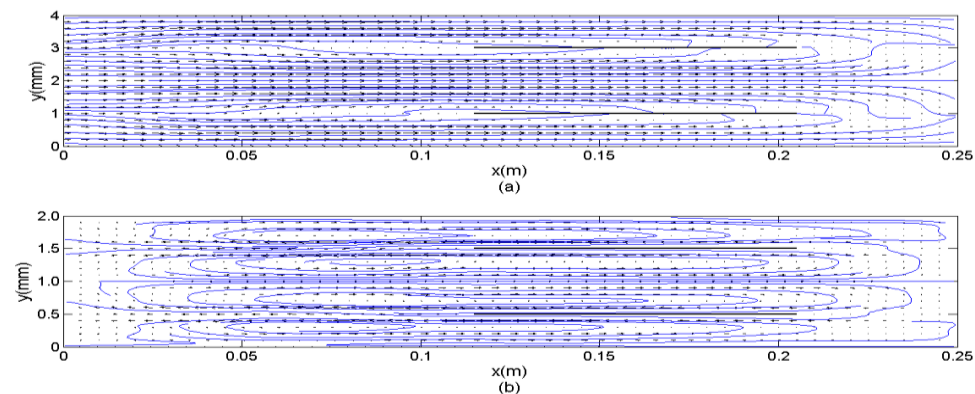
Figure 8 Vector plot and streamline for Case 5 at (a) 7T/16 and (b) 8T/16
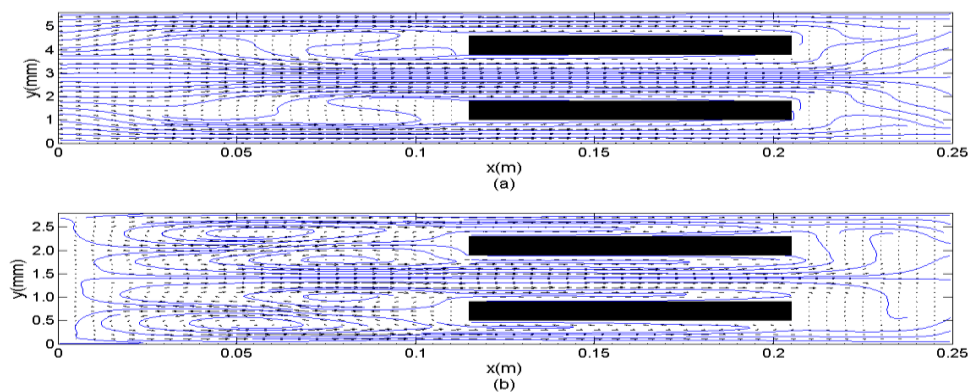
Figure 9 Vector plot and streamline for Case 6 at (a) 7T/16 and (b) 8T/16

The vector plots and streamlines confirmed what were observed with the single plate simulation. In addition, more details are seen particularly in the streaming close to the plate walls. For the negligible thickness plate shown in Figure 8, streamlines are almost uniform,

showing that plate thickness greatly affects the streaming, which tends to reduce the thermoacoustic effects. With the 0.8 mm thick plate, the presence of additional vortices is observed, compared to the 0.4 mm thick plate, in the direction of the driver.

The next case investigated is the plate separation gap where the recommended distance of 2–4 times the thermal penetration depth is followed (Ke et.al., 2010). Figures 4 through 9 have been obtained with a separation gap of 5 times the thermal boundary layer, δ_k. Figure 10 shows the result with a plate separation distance of $4\delta_k$. Before the half cycle, streamlines between the plates are uniform with streaming effects still observed. In Figure 11, with simulation of $3\delta_k$ layer between the stack plates, elongated vortices can barely be discerned between the two-stack regions. It is believed that with larger distances between the walls, returning particles have the momentum to encourage separated vortices. Smaller distances tend to elongate the ones developed.
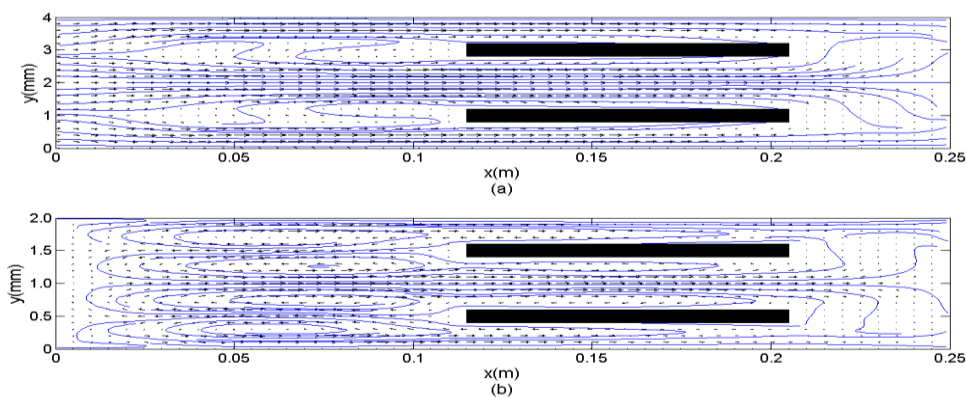
Figure 10 Vector plot and streamline for Case 7 at (a) 7T/16 and (b) 8T/16
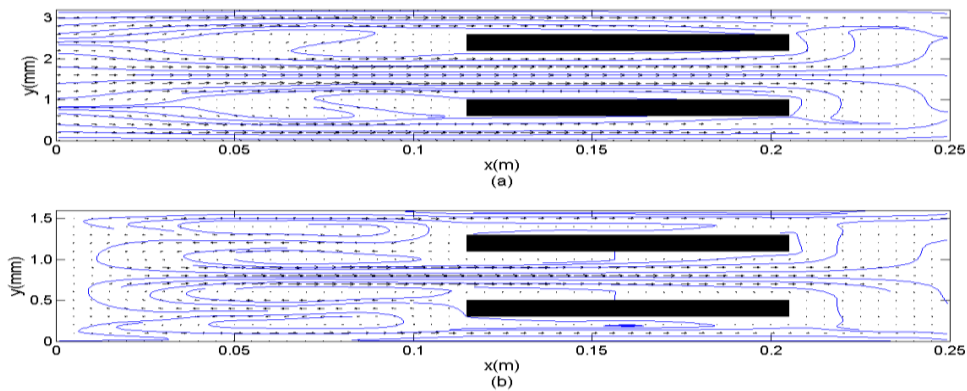
Figure 11 Vector plot and streamline for Case 8 at (a) 7T/16 and (b) 8T/16

The temperature developments are shown in Figures 12 through 14 for the three different thicknesses of the single plate domain investigated. A temperature gradient along the plate is seen at the cycles shown. It seems that higher temperature is located within the vortices. Mixing within these regions induces a higher temperature which is most prominent in Figure 14. Results with a smaller plate separation gap, but still within the recommended limit of $2\delta_k$–$4\delta_k$, show a higher temperature gradient within the gap.
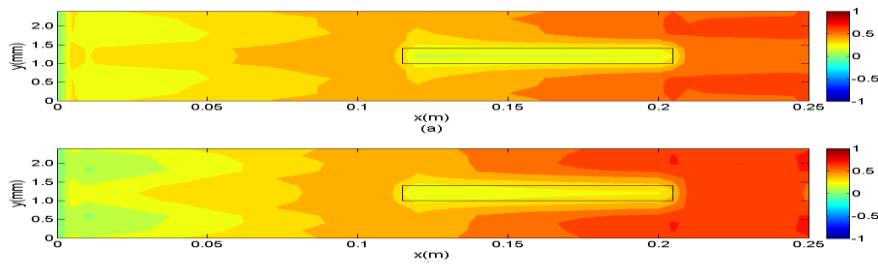
Figure 12 Temperature contour Case 1 at (a) 7T/16 and (b) 8T/16
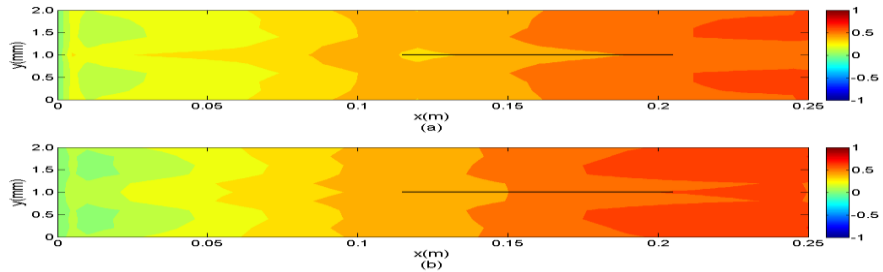
Figure 13 Temperature contour for Case 2 at (a) 7T/16 and (b) 8T/16
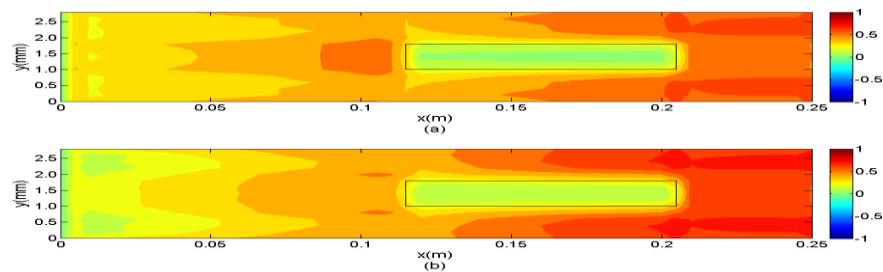
Figure 14 Temperature contour Case 3 at (a) 7T/16 and (b) 8T/16

The differences in temperature development can be seen in Figures 15 through 17. Thus, although thermoacoustic effects still occur next to the plates, reducing the separation gap means more solid walls per unit volume, which translates into an increase in the cooling effects desired. The completed simulation results have shown the individual effects of the parallel plate thickness and separation on the flow and temperature developments of the regions surrounding the plates. Vortices and streaming are almost always present, their strengths dependent greatly on the plate thickness and gap. These are factors that affect the desired cooling expected with the design and tests of a standing wave thermoacoustic refrigerator causing the reasonably low performance. However, due to the absence of any refrigerants or a compressor, the environmentally friendly system is still much sought after in the global agenda towards a more sustainable future.
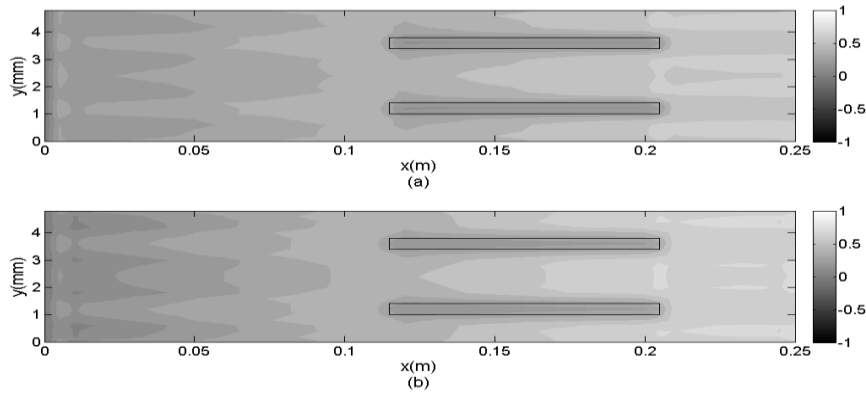
Figure 15 Temperature contour Case 4 at (a) 7T/16 and (b) 8T/16
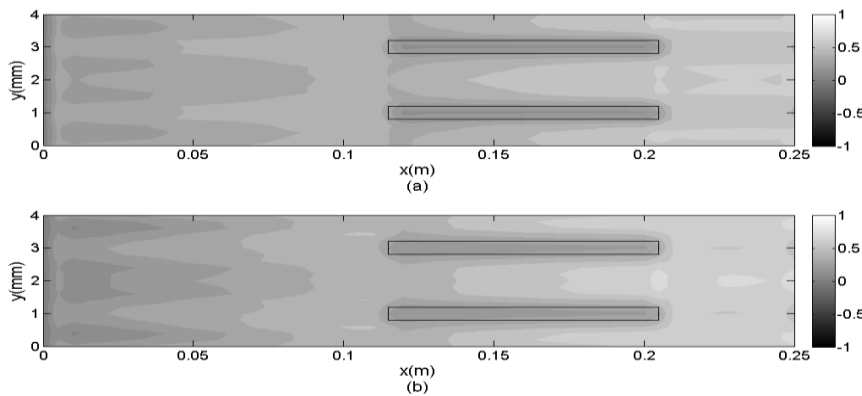
Figure 16 Temperature contour Case 7 at (a) 7T/16 and (b) 8T/16
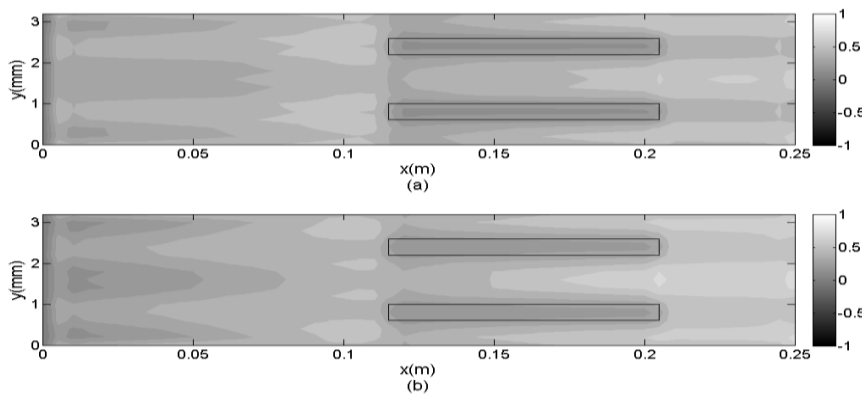
Figure 17 Temperature contour for Case 8 at (a) 7T/16 and (b) 8T/16

4. CONCLUSION

The simulation of the fluid flow and temperature around the parallel stack unit has been completed using the finite difference method with different stack thickness and gap. The developments of the velocity and temperature profiles have shown the existence of vortices and streaming effects. Their presence is very much dependent on the plate thickness and separation gap. Some of key features observed are: (1) Vortices and streaming are always present when acoustic waves pass by the stack of parallel plates, even with a negligible plate thickness modeled; (2) The streamlines are more uniform around a negligible plate thickness. This shows that besides eliminating the undesirable temperature gradient across its thickness, a very thin plate reduces the disturbance to the oscillating fluid as most assumptions have been based on;

(3) Thick plates tend to encourage end vortices as the fluid exits and enters the stack channels and these regions have a higher temperature than the rest, which could also affect the overall thermoacoustic performance; (4) A higher temperature gradient is observed within the gap when the plate separation is within the recommended distance of 2-4 times δ_k.

The simulation described here, however, has neglected the viscous effects that may provide a more significant contribution to the solid walls of the parallel plates towards the development and shedding of vortices as well as exhibiting a more refined streaming effect. In addition, exploration with a finer system of grids close to the plates could possibly be verified, if additional tiny vortices are present within the boundary layer, which could affect the thermoacoustic cooling desired, but this was not attained as expected in the research.

5.   ACKNOWLEDGEMENT

6.   REFERENCES

Abd El-Rahman, A.I., Abdel-Rahman, E., 2013. Computational Fluid Dynamics Simulation of a Thermoacoustic Refrigerator. *Journal of Thermophysics and Heat Transfer,* Volume 28(1), pp. 78−86

Blanc-Benon, P., Besnoin, E., Knio, O., 2003. Experimental and Computational Visualization of the Flow Field in a Thermoacoustic Stack. *Comptes Rendus Mecanique,* Volume 331(1), pp. 17−24

Cao, N., Olson, J.R., Swift, G.W., Chen, S., 1996. Energy Flux Density in a Thermoacoustic Couple. *The Journal of the Acoustical Society of America,* Volume 99(6), pp. 3456−3464

Galioulinna, E., Renterghem, T.V., Botteldooren, D., 2005. 3D Numerical Model of Secondary Streaming in an Acoustic-Resonance Tube Refrigerator. In: *Proceedings of the Twelfth International Congress on Sound and Vibration* (ICSV12), 11−14 July, 2011, Lisbon, Portugal

Ishikawa, H., Mee, D.J., 2002. Numerical Investigations of Flow and Energy Fields near a Thermoacoustic Couple. *The Journal of the Acoustical Society of America,* Volume 111(2), pp. 831−839

Ke, H.B., Liu, Y.W., He, Y.L., Wang, Y., Huang, J., 2010. Numerical Simulation and Parameter Optimization of Thermo-acoustic Refrigerator Driven at Large Amplitude. *Cryogenics,* Volume 50(1), pp. 28−35

Liew, K.F., 2015. Simulation of the Fluid Flow around the Stack Unit in a Thermoacoustic Resonator. B.Eng (Mechanical) Thesis. Universiti Teknologi Malaysia, Malaysia

Marx, D., Blanc-Benon, P., 2004. Numerical Simulation of Stack-heat Exchangers Coupling in a Thermoacoustic Refrigerator. *AIAA Journal,* Volume 42(7), pp. 1338−1347

Mohd. Ghazali, N., 2001. *Numerical Simulation of Acoustic Waves in a Rectangular Chamber.* University of New Hampshire, USA

Shi, L., Yu, Z.B., Jaworski, A.J., 2010. Vortex Shedding Flow Patterns and their Transitions in Oscillatory Flows Past Parallel-plate Thermoacoustic Stacks. *Experimental Thermal and Fluid Science,* Volume 34(7), pp. 954−965

Tijani, M.E.H., 2001. *Loudspeaker-driven Thermo-acoustic Refrigeration*: Technische Universiteit Eindhoven Eindhoven, Netherlands

Worlikar, A.S., Knio, O.M., 1996. Numerical Simulation of a Thermoacoustic Refrigerator: I. Unsteady Adiabatic Flow around the Stack. *Journal of Computational Physics,* Volume 127(2), pp. 424−451

Liew & Mohd-Ghazali 583

Zhang, D.W., He, Y.L., Yang, W.W., Wang, Y., Tao, W.Q., 2013. Particle Image Velocimetry Measurement on the Oscillatory Flow at the End of the Thermoacoustic Parallel Stacks. *Applied Thermal Engineering,* Volume 51(1–2), pp. 325–333

Zoontjens, L., Howard, C.Q., Zander, A.C., Cazzolato, B.S., 2009. Numerical Study of Flow and Energy Fields in Thermoacoustic Couples of Non-zero Thickness. *International Journal of Thermal Sciences,* Volume 48(4), pp. 733–746